Evolution of lithium ordering with (de)-lithiation in β-LiVOPO4: Insights through solid state NMR and first principles DFT calculations

Journal:	*Journal of Materials Chemistry A*
Manuscript ID	TA-ART-01-2020-000121.R1
Article Type:	Paper
Date Submitted by the Author:	19-Feb-2020
Complete List of Authors:	Britto, Sylvia; University of Cambridge, Department of Chemistry; Diamond Light Source Ltd Seymour, Ieuan; University of Cambridge, Department of Chemistry; University of Texas at Austin, The Department of Chemistry and the Institute for Computational Engineering and Sciences Halat, David; University of Cambridge, Department of Chemistry; University of California Berkeley Hidalgo, Marc F.; Binghamton University, Materials Science and Engineering Siu, Carrie; State University of New York at Binghamton, Reeves, Philip; Cambridge University, Department of Chemistry Zhou, Hui; State University of New York, Binghamton Chernova, Natasha; Binghamton University, Whittingham, M.; Binghamton University, NECCES Grey, Clare; University of Cambridge, Chemistry Department

Evolution of lithium ordering with (de)-lithiation in β-LiVOPO$_4$: Insights through solid state NMR and first principles DFT calculations

Sylvia Britto,[a,ŧ] Ieuan D. Seymour,[a,ǂ] David M. Halat,[a,//] Marc F. V. Hidalgo,[b] Carrie Siu,[b] Philip J. Reeves,[a] Hui Zhou,[b] Natalya A. Chernova, [b] M. Stanley Whittingham[b] and Clare P. Grey[a,]*

[a]Department of Chemistry, University of Cambridge, Lensfield Road, Cambridge CB2 1EW UK.

[b]NorthEast Center for Chemical Energy Storage at Binghamton University, Binghamton, NY13902, USA

Current addresses:
[ŧ] Diamond Light Source Ltd., Harwell Science and Innovation Campus, Didcot, OX11 0DE, U.K
[ǂ]Department of Chemistry and the Institute for Computational Engineering and Sciences, The University of Texas at Austin, Austin, Texas 78712, United States
[//]Dept. of Chemical and Biomolecular Engineering, University of California, Berkeley, CA 94720, U.S
*Corresponding Author

Abstract

The lithium ion battery cathode material β-VOPO$_4$ is capable of intercalating more than one Li ion per transition metal ion due to the accessibility of both the V^{5+}/V^{4+} and V^{4+}/V^{3+} redox couples at ~4.5 V and ~2.3 V vs. Li, respectively, giving a theoretical capacity greater than ~300 mAh g^{-1}. The ability to perform full and reversible two Li-ion intercalation in this material, however, has been a matter of debate and the poor crystallinity of the fully lithiated phase has thus far precluded its complete structural characterization by conventional diffraction-based methods. In this work, ^{7}Li and ^{31}P NMR spectroscopy, in combination with first principles DFT calculations, indicate that chemical lithiation results in a single phase β-Li$_2$VOPO$_4$ exhibiting a complex Li ordering scheme with lithium ions occupying multiple disordered environments. 2D NMR ^{7}Li correlation experiments were used to deduce the most likely Li ordering for the β-Li$_2$VOPO$_4$ phase from amongst several DFT optimised structures. In contrast, electrochemically lithiated β-Li$_{2-x}$VOPO$_4$ discharged to 1.6 V exhibits, in addition to β-Li$_2$VOPO$_4$, a β-Li$_{1.5}$VOPO$_4$ phase. The existence of β-Li$_{1.5}$VOPO$_4$ is not reflected in the flat galvanostatic charge and discharge curves nor is evident from diffraction-based methods due to the very close structural similarity between the β-Li$_{1.5}$VOPO$_4$ phase and β-Li$_2$VOPO$_4$ phases. We demonstrate that solid state NMR spectroscopy, in combination with DFT results provides a powerful tool for identifying intermediate states formed during charge/discharge of these complex phosphates as these phases can be distinguished from the end member phases primarily by the nature of the lithium ordering.

Introduction

Lithium-ion batteries are currently the predominant electrical energy storage technology used to power our portable electronics as well as electric vehicles. However the high cost and limited capacities (~120–180 mAh g^{-1}) of commercial intercalation-based cathode materials such as $LiCoO_2$, $LiNi_{1-x-y}Co_xAl_yO_2$ (NCA) and $LiNi_xMn_yCo_zO_2$ (NCM, $0 \leq x,y,z < 1$)[1–9] has restricted their use in large-scale applications such as grid-scale energy storage. Phosphate-based cathode materials primarily represented by $LiFePO_4$[10–14] have offered a promising alternative to the oxides as the inductive effect of the PO_4^{3-} group allows for high voltage (>3.4 V) charging without the structural instability at high voltages often observed with the oxide based cathodes.[15–17] However, the capacity of $LiFePO_4$ is still limited to ~170 mAh g^{-1} due to the one-electron Fe^{2+}/Fe^{3+} couple and limited sites for Li within the olivine structure. The vanadyl phosphates, Li_xVOPO_4, offer the advantage of both high voltage as well as allowing for two-electron reduction giving rise to theoretical specific capacities of ~300 mAh g^{-1} due to the accessibility of both the $V^{3+/4+}$ as well as the $V^{4+/5+}$ redox couples.

The vanadyl phosphates exhibit diverse polymorphism with 7 different polymorphic modifications known to date.[18–23] However only the α_1, β and ε polymorphs have been serious contenders as lithium-ion battery materials, owing in part to the difficulty in synthesising the other polymorphs as single-phase materials free of impurities. The α_1 polymorph is a layered (2D) phase, whereas both the β and ε polymorphs have 3D structures comprising VO_6 octahedra bridged by PO_4 groups. For example, the structure of β-$LiVOPO_4$, the material studied in this work, comprises VO_6 octahedra corner-shared with adjacent VO_6 octahedra along the [100] direction and bridged by PO_4 groups both along the *b* and *c* directions to form a 3D framework of VO_6 octahedra bridged by PO_4 groups (Figure 1(a)). The Li ions are located in octahedral sites that share two faces with VO_6 octahedra and form 1D diffusion channels along the [010] direction.

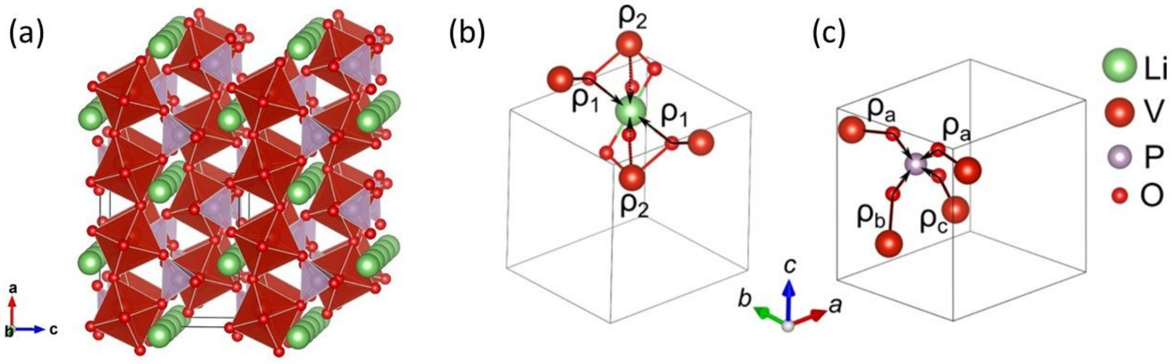

Figure 1. (a) Structure of β-$LiVOPO_4$ along the *b*-direction, (b) local coordination environment around the single Li octahedral site in β-$LiVOPO_4$ and (c) local coordination environment around the phosphorus tetrahedral site in β-$LiVOPO_4$. V-O-Li and V-O-P bond pathways (ρ_i), used to help interpret the ^{7}Li and ^{31}P NMR spectra, as given in Table 1, are marked in (b) and (c), respectively.

While there are numerous studies on the electrochemical and structural aspects of the α_1 and ε polymorphs,[24–27] much less is known about the mechanism of lithiation of the β phase. Ren et al.[28] have demonstrated the use of β-$LiVOPO_4$ as an anode in lithium-ion batteries and suggested that one Li ion per formula unit can be intercalated into the structure to give Li_2VOPO_4, with deeper discharge down to 0.01 V resulting in the formation of metallic vanadium and Li_3PO_4. Allen et al.[29] have also investigated the electrochemical performance of both ε and β-$LiVOPO_4$ and the evolution of the local geometry of the VO_6 octahedra with electrochemical cycling using X-ray spectroscopic techniques. More recently, Harrison et al.[30] have studied the phases formed on electrochemical and chemical lithiation of α- and β-$LiVOPO_4$ using mainly X-ray and neutron diffraction as well as X-ray spectroscopy methods. They suggest a two-phase mechanism operating upon lithiation of β-$LiVOPO_4$, with the plateau in the galvanostatic charge curve at ~2 V arising due to equilibrium between a two-phase mixture of β-$LiVOPO_4$ and β-Li_2VOPO_4.

Lin et al. carried out a combined first-principles and experimental investigation that examined the relative thermodynamic stability, voltages, band gaps and diffusion kinetics for alkali intercalation into the α_1, β and ε polymorphs of $VOPO_4$.[31] They constructed a 0 K calculated phase diagram for A_xVOPO4 (x = Li and Na), suggesting that for the β polymorph, an intermediate phase exists for x = 1.5; however, no clear experimental evidence for the formation of this phase during electrochemical cycling was found. Moreover, the poor crystallinity of the electrochemically- as well as the chemically-lithiated phases precluded a detailed structure solution of β-Li_2VOPO_4.

Despite the utility of X-ray diffraction-based crystallographic methods to investigate the lithiation mechanisms in battery materials, these methods give limited insights as to the evolution of lithium ordering with electrochemical cycling, an understanding of which is crucial to reveal the influence of structure on the electrochemical performance. Solid-state NMR spectroscopy remains one of the few techniques capable of probing lithium ordering and dynamics in the often poorly crystalline phases formed during the electrochemical cycling. In this work, we carry out a detailed ^7Li and ^{31}P NMR and first principles calculations study to gain insights into the lithium ordering in the pristine as well as electrochemically - and chemically-lithiated forms of β-$LiVOPO_4$. Both the ^7Li as well as ^{31}P NMR data clearly indicate formation of an intermediate $Li_{1.5}VOPO_4$ phase during the discharge process; the assignments of the NMR spectra are supported by first principles calculations of both the energetics of different lithium ordering schemes of the $Li_{1+x}VOPO_4$ phases and their associated ^7Li and ^{31}P hyperfine shifts. The results indicate that the discharge process is not a simple two-phase transformation between $LiVOPO_4$ and Li_2VOPO_4 but involves an intermediate, partially-lithiated metastable phase that is not readily observable by long range characterization techniques such as X-ray diffraction (XRD).

Experimental

Synthesis of Materials: β-$LiVOPO_4$ was synthesised through the calcination of a hydrothermally synthesised precursor, $LiVOPO_4{\cdot}2H_2O$.[32] The precursor was prepared by first stirring V_2O_5 (Aldrich, >99.6%), oxalic acid (Sigma-Aldrich, >99.0%), and phosphoric acid (Fisher Scientific, 85%) for 18 hours in water and ethanol (in 3:1 volume ratio), followed by the addition of $LiOH{\cdot}H_2O$ (Sigma, >99.0%) and an additional 4 hours of stirring. The solution was then placed in a 4748 Type 125 mL PTFE-lined reactor (Parr Instrument Co.) and heated to 160 °C for 48 hours. The resulting $LiVOPO_4{\cdot}2H_2O$ was then filtered, dried, and heated (calcined) at 600 °C in O_2 for 3 hours to form β-$LiVOPO_4$.

β-$VOPO_4$ was synthesised by calcining a H_2VOPO_4 precursor. The precursor was prepared by dissolution of VCl_3 (Sigma-Aldrich, 97%) and P_2O_5 (Sigma-Aldrich, ≥98%) in 190 proof ethanol (Pharmco-AAPER), which was placed in a 4748 Type 125 mL PTFE-lined reactor (Parr Instrument Co.) and heated to 180 °C for 72 hours. The resulting precursor was extracted through centrifugation and heated (calcined) at 700°C for 3 hours.

Diffraction: All precursors and the final product β-$LiVOPO_4$ and β-$VOPO_4$ were characterized by powder XRD using a Bruker D8 Advanced X-ray diffractometer equipped with a Cu Kα source, $\lambda = 1.54178$ Å. The diffraction patterns were recorded within the 2θ range from 10° to 80° with 2θ steps of 0.02°. The unit cell parameters were obtained by Rietveld refinement using the diffraction patterns within the TOPAS program.

Electrochemical testing: β-$VOPO_4$ and β-$LiVOPO_4$ were electrochemically (de)lithiated by using the materials as cathodes in 2325-type coin cells. β-$LiVOPO_4$ was first subjected to high-energy ball-milling with graphene for 30 minutes. Polyvinylidene fluoride (PVDF) was then added to the mixture, resulting in a β-$LiVOPO_4$:graphene:PVDF ratio of 75:15:10. This mixture was formed into a slurry with n-methyl-2-pyrrolidinone (NMP) as the solvent, doctor blade coated onto a carbon-coated Al foil, and dried at 60 °C. Electrodes with an area of 1.2 cm^2 were punched from the dried slurry, with resultant mass loadings of ~2.5–4.5 mg. Cells were then assembled using the prepared electrodes as the cathode, a pure lithium chip (MTI) as the counter and reference electrodes, a Celgard 2400 separator (Hoechst Celanese) as the separator, and 1 M $LiPF_6$ in 1:1 v/v ethylene carbonate (EC) and dimethyl carbonate (DMC) as the electrolyte. Electrochemical (de)lithiation of the β-$LiVOPO_4$ and β-$VOPO_4$ was conducted at C/100 (C = 318 mAh g^{-1}). Galvanostatic intermittent titration technique (GITT) measurements of β-$LiVOPO_4$ were conducted by discharging the cell at a rate of C/100 for 1.5 hours followed by a relaxation period of 100 hours.

Chemical lithiation: Chemical lithiation was performed with *n*-butyllithium as the reducing agent. *N*-butyllithium and the synthesised pure β-$LiVOPO_4$ sample (in a 1:1 molar ratio) were mixed in hexane and stirred for 3 days. After reaction, the chemically-lithiated product was rinsed with hexane 3 times and collected through filtration. The mixing, stirring and sample collection steps were carried out inside an Ar-filled glovebox to avoid sample exposure to air.

Solid-state NMR: ^7Li and ^{31}P NMR experiments were acquired with a Bruker 1.3 mm HX probe using a 4.7 T (200 MHz) magnet. Spectra were acquired at Larmor frequencies of 77.77 MHz and 81.04 MHz for ^7Li and ^{31}P, respectively. ^7Li 1D spectra were acquired using a rotor-synchronised Hahn echo pulse sequence at a magic-angle spinning (MAS) rate of 60 kHz with a $\pi/2$ pulse length of 1.02 μs at a power level of 43.5 W, initially optimised on an external reference of Li_2CO_3 (referenced to 1.1 ppm). ^{31}P spectra were acquired, also at a MAS rate of 60 kHz, using a $\pi/2$ pulse length of 0.75 μs at a power level of 53 W, externally referenced to ammonium dihydrogen phosphate ($NH_4H_2PO_4$) at 1.0 ppm. 2D permutationally offset stabilised C7 (POST-C7) ^7Li spectra[33–35] were acquired using a spinning speed of 63 kHz, which was chosen to correlate the full range of features observed. The POST-C7 experiments used 9 composite C7 cycles for double quantum excitation and reconversion, corresponding to an evolution time of 0.57 ms; the recycle delay was 40 ms and the RF power level was set the same as for the 7Li 1D spectra. 2D exchange spectroscopy (EXSY) ^7Li measurements[36–38] were performed also using a spinning speed of 63 kHz; the mixing period was 8 ms and the recycle delay was 50 ms.

Computational methods: Solid-state hybrid density functional theory (DFT) calculations were performed using CRYSTAL14,[39] a linear combination of atomic orbitals (LCAO) code. All calculations were performed using the PBE0 hybrid functional[40] with a total energy convergence criteria of 2.72×10^{-6} eV, a Monkhorst-Pack mesh of 8×8×8 and integral tolerances of 10^{-7}, 10^{-7}, 10^{-7}, 10^{-7} and 10^{-14} as defined in the CRYSTAL14 documentation. The atomic positions and lattice parameters of different Li_xVOPO_4 structures (x = 1, 1.5 and 2), taken from a previous DFT study,[25] were optimised using a quasi-Newtonian algorithm. RMS convergence criteria of 8.16×10^{-3} and 3.27×10^{-2} eV were adopted for forces and displacements respectively. All calculations were performed in the spin polarised, ferromagnetic state unless otherwise stated.

The ^7Li and ^{31}P Fermi contact shifts were calculated for the geometry-optimised structures using the method developed in previous studies[41–43]; only a brief summary is given here. It has been shown in previous work that hybrid functionals are required to accurately describe the Fermi contact interactions in paramagnetic materials.[42,44] The size of the Fermi contact shift is sensitive to the percentage of Fock exchange (F_0) included in the hybrid functional, with F_0=20% and 35% representing the upper and lower bounds, respectively, of experimentally observed shifts. In this work, the PBE0 hybrid functional with F_0 = 25% was therefore also adopted for the calculations of Fermi contact shifts.

For geometry optimisations, a small, contracted basis set (BS-I) was used which was taken unmodified from the CRYSTAL online repository. BS-I had the form (7s2p1d)/[1s2sp1d] for Li, (20s12p4d)/[1s4sp2d] for V, (10s4p1d)/[1s2sp1d] for O, and (16s8p1d)/[1s3sp1d] for P, where the values in parentheses denote the number of Gaussian primitives and the values in square brackets denote the contraction scheme. For the calculation of Fermi contact shifts, a more extended basis set (BS-II) was used which had the form (9s2p)/[5s2p] for Li, (13s9p5d)/[7s5p3d] for V, (10s6p2d)/[6s5p2d] for O and (11s7p3d)/[7s6p3d] for P. The BS-II in this work has also previously been used to calculate the Fermi contact shifts of Fe phosphates, [42,44] Li_2VO_2 [35] and ε-$LiVOPO_4$.[45]

Calculation of ^7Li and ^{31}P Fermi contact shifts: Fermi contact shifts of the pristine Li_xVOPO_4 structures were calculated with single point energy calculations using the BS-II basis set. In order to scale the Fermi contact shifts calculated from DFT at 0 K in the ferromagnetic state into the paramagnetic regime, the previously-reported approach was adopted,[42,44] in which the DFT calculated hyperfine coupling constant, A_{iso}, was multiplied by a magnetic scaling factor, Φ, defined as:

$$\Phi = \frac{B_0\mu_{eff}^2}{3k_B g_e \mu_B S_{form}(T-\theta)} \qquad (1)$$

where B_0 is the external magnetic field, k_B is the Boltzmann constant (1.381×10^{-23} J K^{-1}),, g_e is the free electron *g* factor (equal to 2.0023), μ_B is the Bohr magneton (9.274×10^{-24} J T^{-1}), T is the experimental temperature at which the NMR spectra were recorded, μ_{eff} is the effective magnetic moment and θ is the Weiss constant. S_{form} is the formal spin angular momentum quantum number which is equal to ½ and 1 for V^{4+} and V^{3+}, respectively. Based on previous magnetic measurements of $LiVOPO_4$[46] μ_{eff} was taken as the spin-only magnetic moment for V^{4+} (1.732 μ_B) and V^{3+} (2.828 μ_B) The Weiss constant, θ, was taken to be 0 K (i.e. the Curie spin approximation), which is an approximation for the weakly antiferromagnetic Weiss constant of -67.5 K measured for $LiVOPO_4$[46]The value of T was taken as 340 K to account for frictional heating due to the MAS rate of 60 kHz. The scaling factors for V^{4+} and V^{3+} were 9.29×10^{-3} and 12.28×10^{-3}, respectively, from Equation 1.

The total Fermi contact shift (δ_i) for individual ^7Li and ^{31}P sites (i) was decomposed into the separate Li-O-V and P-O-V bond pathway contributions (ϱ_n) using the spin-flipping method of Middlemiss et al.[43] In this approach, the difference between the Fermi contact shift on a given $^7Li/^{31}P$ site is calculated for ferromagnetic and ferrimagnetic spin alignments of neighbouring V sites. The individual ϱ_i bond pathway contributions from the n neighbouring

V sites can be summed to recover the total shift $\delta_i = \sum_n \varrho_n$. For the $Li_{1.5}VOPO_4$ structures with mixed V^{4+}/V^{3+} sites, before summation, the individual ϱ_i contributions were scaled by the appropriate V^{4+} or V^{3+} scaling factor depending on the oxidation state of the V ion involved in the spin density transfer.

Results

Ab-initio DFT studies of the pristine and lithiated samples: DFT calculations were first performed in order to explore the energetics and to assign the experimental NMR shifts to specific sites in the phases formed during electrochemical lithiation of β-$LiVOPO_4$. These studies build on the DFT results for β-$LiVOPO_4$ previously reported,[31] in addition to calculating the NMR hyperfine shifts to make connections with experiment.

β-$LiVOPO_4$ exhibits a single octahedrally-coordinated Li environment (Figure 1 (a) and Figure 2(a)) surrounded by tetrahedral and distorted octahedral vacancies. In prior work,[31] different configurations were produced by populating the vacant sites with Li ions, which were subsequently relaxed with Hubbard U-corrected DFT calculations (DFT+U) to produce a convex energy hull. As a starting point for the calculations in the present study, the lowest energy structures on the hull at lithium compositions of β-Li_xVOPO_4, where x = 1, 1.5 and 2, were investigated, in addition to several configurations that were close in energy to the hull structures. These structures are given in Table SI. 1-5 and depicted in Figure 2. In all cases, the structures obtained from the hull were fully optimised using the PBE0 functional within the CRYSTAL14 code before calculation of the NMR parameters. . A density of states plot for each of the lowest energy LixVOPO4 structures (x =1, 1.5 and 2) calculated with PBE0 is shown in SI. 1.

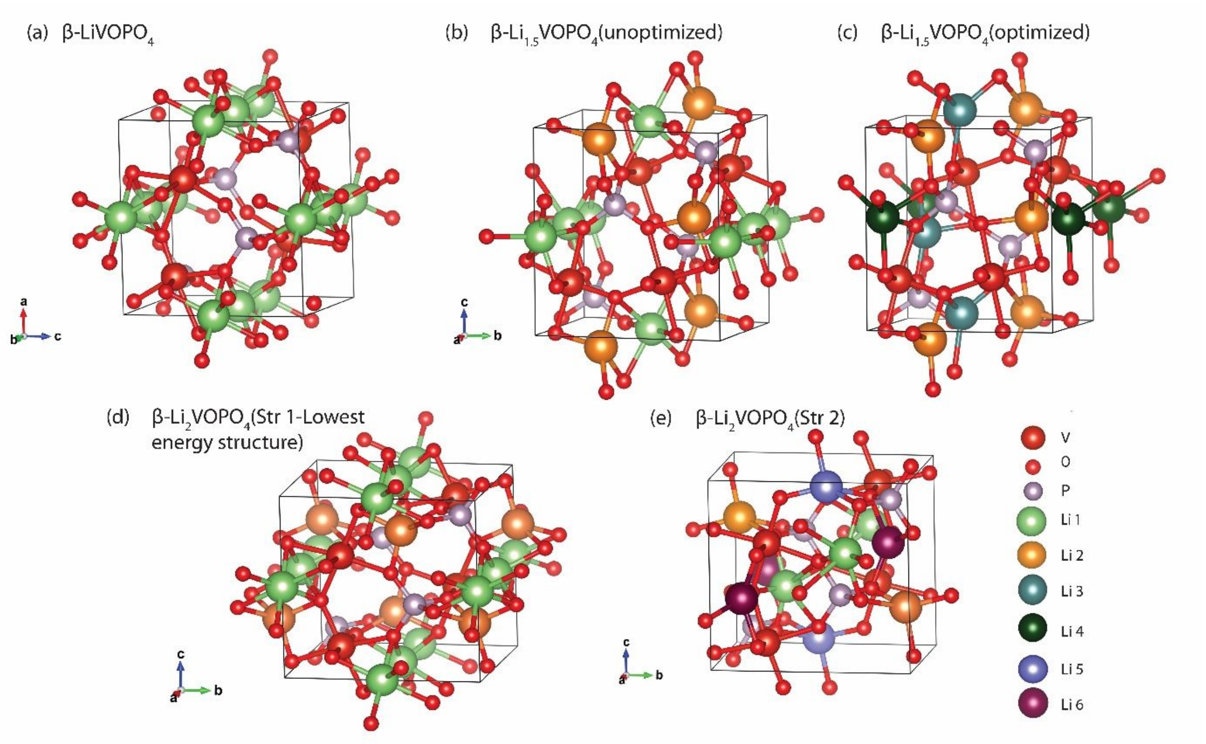

Figure 2. Crystal structure of (a) β-$LiVOPO_4$, (b) β-$Li_{1.5}VOPO_4$ (before optimization), (c) β-$Li_{1.5}VOPO_4$ (after optimization), (d) β-Li_2VOPO_4 (Str 1) (lowest energy structure) and (e) β-Li_2VOPO_4 (Str 2). The structure of β-$LiVOPO_4$ is shown to allow for comparison with the other more highly lithiated phases.

In the three lowest energy structures of $Li_{1.5}VOPO_4$ reported in the previous study,[31] the excess Li ions occupied tetrahedral sites (Li 2) on either side of the octahedral sites present in the $LiVOPO_4$ structure as shown in Fig 2(b). During the full structural optimisation of the lowest energy $Li_{1.5}VOPO_4$ structure on the hull, significant relaxation of the initial octahedral Li positions (Li 1) occurred resulting in the migration of 50% of the octahedral sites to adjacent tetrahedral sites (Li3) and the other 50% to neighbouring distorted octahedral sites (Li 4) (Figure 2(b)). The Li ions in tetrahedral sites in the initial unoptimised structure (Li 2) remained on the same site after optimisation, although there was a small distortion of the Li position from the centre of the LiO_4 tetrahedra. For the other two structures near the hull, the final structures after relaxation contained Li ions in the undistorted octahedral and tetrahedral sites that were present in the initial structures. The two near hull structures were 136 and 202 meV per f.u. higher in energy than the ground state structure. It can be concluded therefore that lithiation beyond x = 1 results in a significant displacement of the initial octahedral Li sites, as well as occupation of new environments.

The lowest energy structure of Li_2VOPO_4 (Str 1) has full occupation of the tetrahedral sites adjacent to the octahedral sites in $LiVOPO_4$ structure (Figure 2(c)). A slightly higher energy (56 meV per f.u.) Li_2VOPO_4 structure (Str 2) was also investigated, which contained Li in additional tetrahedral and distorted octahedral sites (Li 5 and Li 6) that were not present in the lowest energy structure to explore potential Li disorder. The ^{7}Li and ^{31}P NMR hyperfine shifts of all of the phases are shown in Figure 3. Of note, the tetrahedrally coordinated Li sites all exhibit zero or positive shifts, while the octahedrally coordinated shifts show either negative or very small positive shifts; these hyperfine shifts are analysed in more detail after the experimental NMR results are presented.

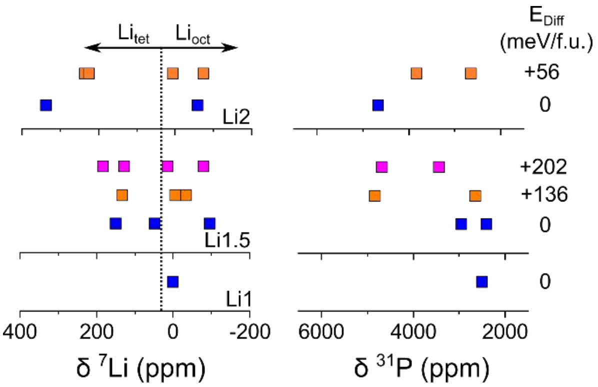

Figure 3. DFT-calculated (a) ^{7}Li and (b) ^{31}P Fermi contact NMR shifts for low energy Li_xVOPO_4 ($x = 1$, 1.5 and 2) structures. The DFT energies of the structures relative to the lowest energy structure at each composition (E_{Diff}) is given in meV per f.u. The ^{7}Li shift ranges of tetrahedral (Li_{tet}) and octahedral (Li_{oct}) sites from x = 1-2 is indicated. All shifts were scaled to 340 K assuming a spin-only magnetic moment.

Experimental NMR spectra of pristine β-LiVOPO$_4$: The ^{7}Li NMR spectrum of pristine β-$LiVOPO_4$ exhibits a single isotropic shift at 3 ppm (Figure 4(a)) consistent with the one crystallographic site for lithium in the structure (Figure 1b and Figure 3). In general, the $^{6/7}Li$ chemical shift range of diamagnetic compounds lies from 0 to ±5 ppm, whereas paramagnetic materials generally exhibit much larger shifts due to the Fermi contact interaction that arises due to the transfer of spin density from the paramagnetic center (in this case, V^{4+} in the $t_{2g}^{1}e_{g}^{0}$ electronic configuration) to the NMR active nucleus through the intervening oxygen atoms.

Thus, the observation of a shift near 0 ppm in paramagnetic β-LiVOPO$_4$ is surprising and warrants further exploration.

A better understanding of the ~0 ppm shift can be gained by decomposition of the overall Fermi contact shift calculated above (Figure 3) into its constituent Li-O-V^{4+} bond pathway contributions through a DFT-based bond pathway contribution analysis using the spin flipping approach (for more details see Table 1 and Figure 1(b) and (c)). The lithium ions are connected to two V^{4+} ions through 122.7° Li-O-V^{4+} bond pathways (ρ_1) (see Figure 1(b)), leading to a positive shift contribution of 36 ppm. The LiO$_6$ octahedra also share a common face with two VO$_6$ octahedra through three Li-O-V^{4+} bond overlaps, with angles from 80.1 to 91.4°. The sum of the individual Li-O-V^{4+} bond overlaps (ρ_2), in addition to the direct transfer of spin density from V^{4+} to Li$^+$, leads to a negative shift contribution of -36 ppm per ρ_2 pathway. The sum of the positive and negative pathways contributions for ρ_1 and ρ_2 leads to a net calculated ^{7}Li Fermi contact shift for β-LiVOPO$_4$ of 2 × 36+2 × -36 = 0 ppm.

Table 1: DFT calculations of X-O-V^{4+} (X=^{7}Li or ^{31}P) NMR bond pathway contributions (ρ_i) in the β-LiVOPO$_4$ structure at 340 K. The total shift is calculated as the sum of the individual ρ_i. The bond pathways are depicted in Figures 1 (b) and (c).

	Pathway	No. of Pathways	X-O-V^{4+} Angles (°)	X-V^{4+} Distance (Å)	Fermi Contact Shift (ppm)	Total Shift (ppm)
^{7}Li	ρ_1	2	122.7	3.288	36	0
	ρ_2	2	80.11, 85.15, 91.44	2.828	-36	
^{31}P	ρ_a	2	134.23	3.228	1429	2503
	ρ_b	1	130.93	3.260	0	
	ρ_c	1	152.32	3.325	-335	

A single resonance is seen in the ^{31}P NMR spectrum (Figure 4(b)) with a much larger shift of 1926 ppm, consistent with the paramagnetic nature of this compound. The P site is connected to four V^{4+} sites through three different P-O-V^{4+} bond pathways, ρ_a, ρ_b, and ρ_c(see Figure 1 (c). The large, positive shift contribution predicted from first principles from the two ρ_a pathways ($2 \times 1429\ ppm$) compared to the negligible and weakly negative shifts, respectively, of the ρ_b and ρ_c pathways, leads to an overall positive ^{31}P NMR shift (2503 ppm) in reasonable agreement with the experimental value. The overestimation of the ^{31}P shift may be related to the neglect of antiferromagnetic (AF) ordering through the use of a Weiss constant of θ = 0 K for LiVOPO$_4$ in the calculation of Φ (the magnetic scaling factor), which implicitly assumes that AF correlations do not persist near room temperature.

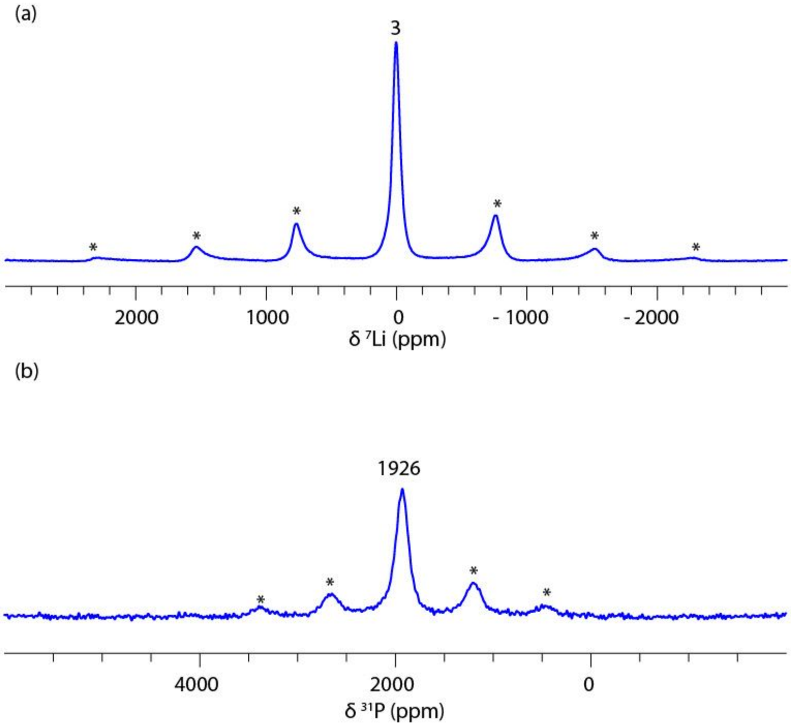

Figure 4. (a) ^{7}Li and (b) ^{31}P NMR spectrum of β-$LiVOPO_4$. All the spectra presented in this work were acquired at a magic angle spinning (MAS) frequency of 60 kHz at 4.7 T unless otherwise noted. Asterisks denote spinning sidebands.

Electrochemistry and NMR characterization of cycling: The galvanostatic charge-discharge curve of β-$LiVOPO_4$ cycled between 1.5 and 4.5 V exhibits an initial sloping region as the material is discharged (lithium insertion) between 3.25 and 2.1 V, before reaching a flat plateau at ~2 V (Figure 5). The GITT (SI. 2) shows that there is a clear plateau at 2.15 V between x = 1.15 and 1.6. At the end of the plateau there is a shallower sloping region between 2.0 V and 1.8 V, which is followed by a steeper sloping region upon discharge to 1.5 V. Discharge to 1.5 V leads to a capacity of ~165 mAh g^{-1} corresponding to intercalation of 1 Li into β-$LiVOPO_4$. On charging, the sloping region is more prominent and is followed by a shorter plateau region at ~2.1 V. The upper voltage region exhibits a single plateau at ~4.0 V which is seen both on charge and discharge.

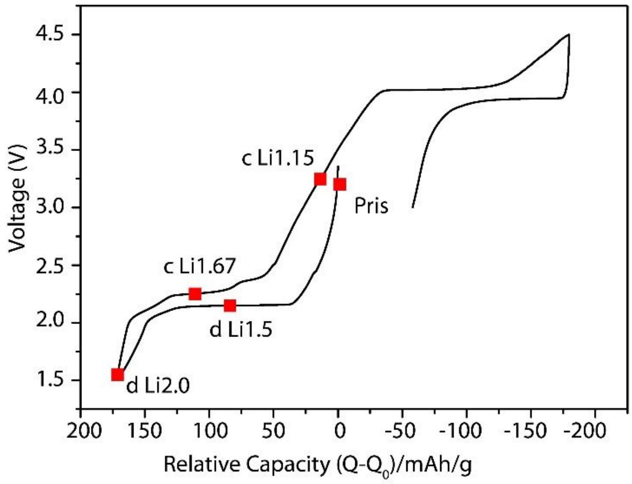

Figure 5. Galvanostatic charge-discharge curve of β-$LiVOPO_4$ cycled between 1.5 V and 4.5 V at a rate of C/50. The points at which *ex-situ* NMR data were acquired are marked. The relative capacity is defined with respect to the pristine β-Li_xVOPO_4 material ($x = 1$).

^{7}Li NMR spectra of β-$LiVOPO_4$ electrodes disassembled at various states of charge (SOC) are shown in Figure 6, and SI. 3. On discharging to 2.1 V (corresponding to a capacity of 89 mAh g^{-1}, or intercalation of 0.5 Li into $LiVOPO_4$), new resonances at 46 ppm as well as a broad environment at 264 ppm are observed. By comparison to the DFT calculations, the appearance of these higher-frequency shifts indicates the onset of Li occupation of distorted "tetrahedral" sites (*e.g.*, Li2 and Li5 sites in Fig 2b, c, and d)) that are not present in the original β-$LiVOPO_4$ structure (Fig 2a).

Using the DFT calculations to aid the assignments, the ^{7}Li shifts close to ~50 ppm arise from local environments in β-$Li_{1.5}VOPO_4$, while the negative shifts and those > 200 ppm are due to octahedral and (highly) distorted "tetrahedral" environments, respectively, in β-Li_2VOPO_4.

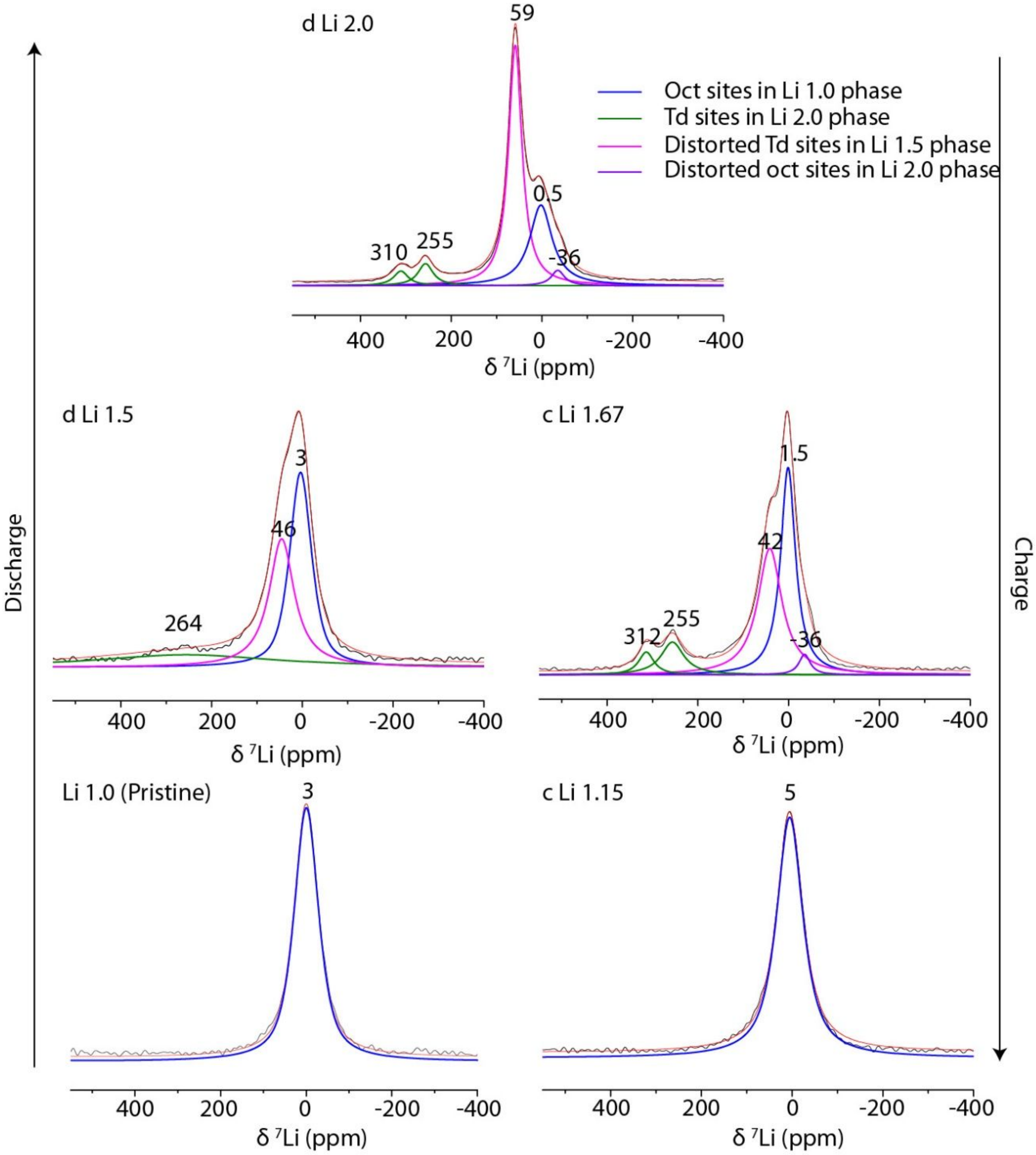

Figure 6. Deconvolution of the ^{7}Li NMR spectra of β-$LiVOPO_4$ cycled to different states of charge (SOC) in the lower voltage region between 3.4 V and 1.5 V. The points in the galvanostatic discharge curve (Li contents) at which the NMR spectra were acquired are as marked in Figure 5. The spectra are scaled arbitrarily.

On charging to 2.1 V (Li 1.67), the relative intensities of the ~3 ppm and ~46 ppm peaks seen in the Li 1.67 spectrum, are similar to those observed on discharge to 2 V (Li 1.5), but the resonances at higher shifts (255 ppm and 310 ppm) remain indicating that Li has not yet been extracted from these distorted "tetrahedral" sites at 2.1 V on charge. ^{7}Li NMR spectra of the electrode obtained on further charging to 3.2 V (Li 1.15) exhibit a single resonance at ~5 ppm due to octahedral Li environments, consistent with reversible formation of the $LiVOPO_4$ phase.

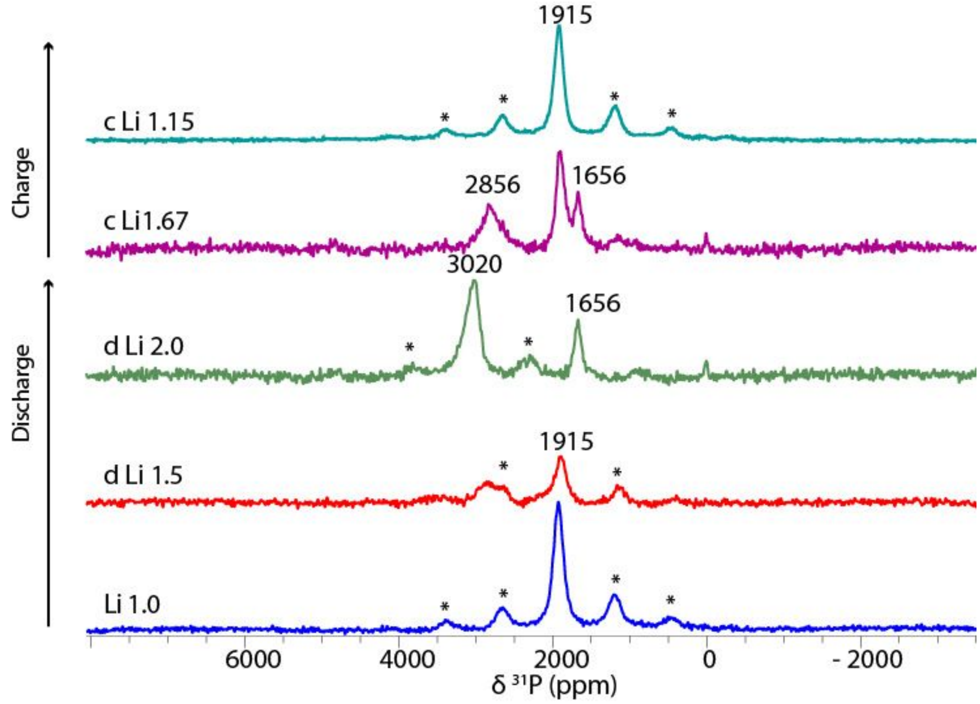

Figure 7. ^{31}P NMR spectra of β-LiVOPO$_4$ cycled to different states of charge (SOC) in the lower voltage region between 3.4 and 1.5 V. The points in the galvanostatic discharge curve that the NMR were acquired at are as marked in Figure 5.

^{31}P NMR spectra of β-LiVOPO$_4$ electrodes disassembled at identical states of charge (SOC) are shown in Figure 7; the electrode samples were the same as those studied by ^{7}Li NMR. On discharging to Li 1.5, in addition to the resonance at ~1915 ppm assigned to LiVOPO$_4$, an additional broad resonance is observed at ~2800 ppm that overlaps with the spinning sideband of the LiVOPO$_4$ phase. Further discharge to 1.5 V (Li 2.0) gives rise to a sharp, well-resolved resonance at 3020 ppm. This is also accompanied by the appearance of a new resonance at 1656 ppm. Therefore, while only one P local environment is predicted for the x = 2 ground state structure, at least two are seen experimentally. However, the calculations also show that there are a variety of lithium orderings in the x = 1.5 and 2.0 compositions that lie close in energy, which appear to be populated under electrochemical cycling.

Upon charging to Li 1.67, the peak at 1656 ppm remains approximately constant in shift, while the resonance originally at ~3100 ppm shifts to ~2850 ppm. In addition, the peak at ~1950 ppm corresponding to the LiVOPO$_4$ phase reappears, confirming that the 1656 and ~1950 ppm peaks originate from different sites. In accordance with the DFT calculations (Fig. 3), the resonances close to 3000 ppm are assigned to the lowest energy structure of β-Li$_{1.5}$VOPO$_4$. Further charging back to ~3.2 V results in disappearance of the peaks at ~2850 and 1656 ppm and growth of the ~1950 ppm peak, confirming delithiation back to the LiVOPO$_4$ phase.

The effect of starting material on lithium ordering:

The experimental ^{7}Li and ^{31}P NMR spectra are not readily explained by one single composition or Li ordering at each state of charge. We now explore whether the method and nature of the starting material play a significant role in the nature of the phase formed. To explore this, and for comparison to prior results,[29,30] a β-VOPO$_4$ sample synthesised by heating tetragonal H$_2$VOPO$_4$ was also discharged to 1.6 V (specific capacity of ~300 mAh g^{-1}; the electrochemistry is shown in SI. 4). The ^{7}Li NMR spectrum of this sample exhibits more intense and sharper peaks at 306 ppm and 258 ppm (Fig. 8(b)) compared to that seen in the sample obtained by discharge of the β-$LiVOPO_4$ precursor (Fig 8(a)).

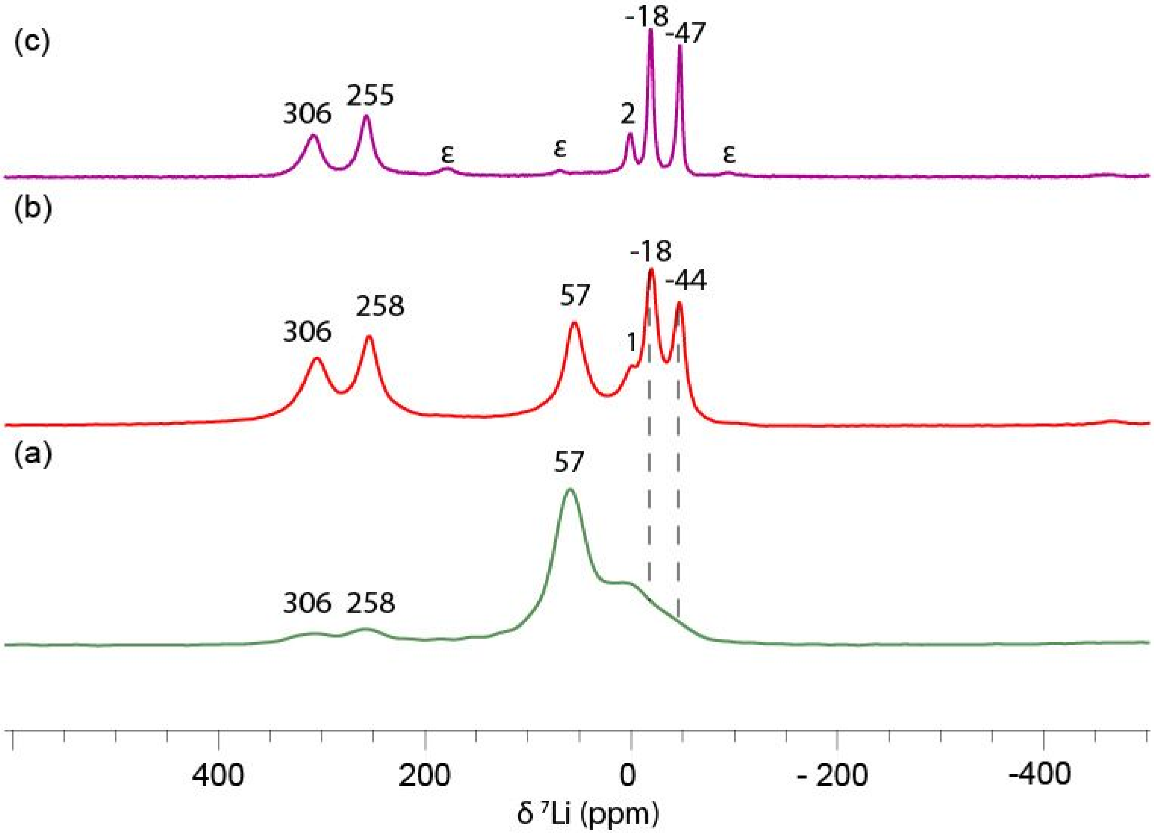

Figure 8. A comparison of the ^{7}Li NMR spectra of (a) β-$LiVOPO_4$ discharged to 1.6 V, (b) β-$VOPO_4$ discharged to 1.6 V, and (c) chemically-lithiated β-Li_2VOPO_4. The minor peaks at ~181 ppm, 71 ppm and −93 ppm in the chemically-lithiated β-Li_2VOPO_4 sample (marked as ε) are assigned to an ε-Li_2VOPO_4 impurity,[47] while that at ~2 ppm is assigned to pristine β-$LiVOPO_4$.

More noteworthy are the more intense and well-resolved peaks observed at −18 and −44 ppm; on the basis of the DFT calculations, these are assigned to Li ions in the environments which are more highly coordinated by O (i.e. Li1 and Li6). Similar to the sample obtained from β-$LiVOPO_4$, this spectrum also exhibits a sharp resonance at ~60 ppm, a feature arising from the β-$Li_{1.5}VOPO_4$ phase. ^{31}P NMR measurements indicate peaks at 4870 ppm, ~3000 ppm and a sharp peak at ~1700 ppm (Fig. 9). Based on DFT (Fig. 3, lowest energy structures), the peak at 4870 ppm is assigned to β-Li_2VOPO_4 while the one at ~3000 ppm is assigned to a β-$Li_{1.5}VOPO_4$ phase. For the sample discharged from $VOPO_4$, the ratio of the integrated intensities of the 4870 ppm peak and the ~1700 ppm peak to the ~3000 ppm peak is 1:0.48, which is in good agreement with the β-Li_2VOPO_4 : β-$Li_{1.5}VOPO_4$ ratio obtained for the same sample from the ^{7}Li NMR (i.e., the 306 ppm + 258 ppm + −18 ppm + −44 ppm : 60 ppm peak ratio is 1:0.41, after normalizing for the expected amount of Li in the phases).

Chemical lithiation with *n*-butyllithium is a well-known method of obtaining stoichiometrically lithiated battery materials.[48] In order to confirm that the shifts obtained at the end of discharge are due to β-Li_2VOPO_4, the NMR spectra of the two electrochemically-lithiated samples are compared with that of chemically-lithiated β-$LiVOPO_4$. The ^{7}Li NMR spectrum of this chemically lithiated sample (Fig. 8(c)) exhibits impurity peaks at 178 ppm, 71 ppm and −93 ppm assigned to ε-Li_2VOPO_4.[47] The peak at ~2 ppm is assigned to the residual β-$LiVOPO_4$ precursor. This leaves the peaks at 306 ppm, 255 ppm, −18 ppm and −47 ppm, which are assigned to Li sites in β-Li_2VOPO_4. The peaks at 306 ppm and 255 ppm are in good agreement with DFT-calculated shifts expected for Li distorted "tetrahedral" environments in the structure of β-Li_2VOPO_4 (Li5 and Li2 sites), while the negative shifts (at −18 ppm and −47 ppm) are in good agreement with DFT calculated shifts expected for Li highly-coordinated environments in the structure of β-Li_2VOPO_4 (the Li1 and Li6 sites). Unlike the electrochemically-lithiated samples, however, the chemically-lithiated sample does not exhibit a peak at ~60 ppm. The corresponding ^{31}P NMR spectrum of the chemically-lithiated sample (Fig.9(c)) also exhibits impurity peaks due to ε-Li_2VOPO_4 at 4352 ppm and 3160 ppm, in addition to the peak due to the precursor β-$LiVOPO_4$ at 1954 ppm. The peak at 4870 ppm is assigned to β-Li_2VOPO_4, in agreement with DFT calculations. This sample also exhibits a sharp resonance at 1678 ppm which is also observed in the electrochemically-lithiated samples discharged to 1.6 V, and which we will assign later after exploring the effect of metastability in the system.

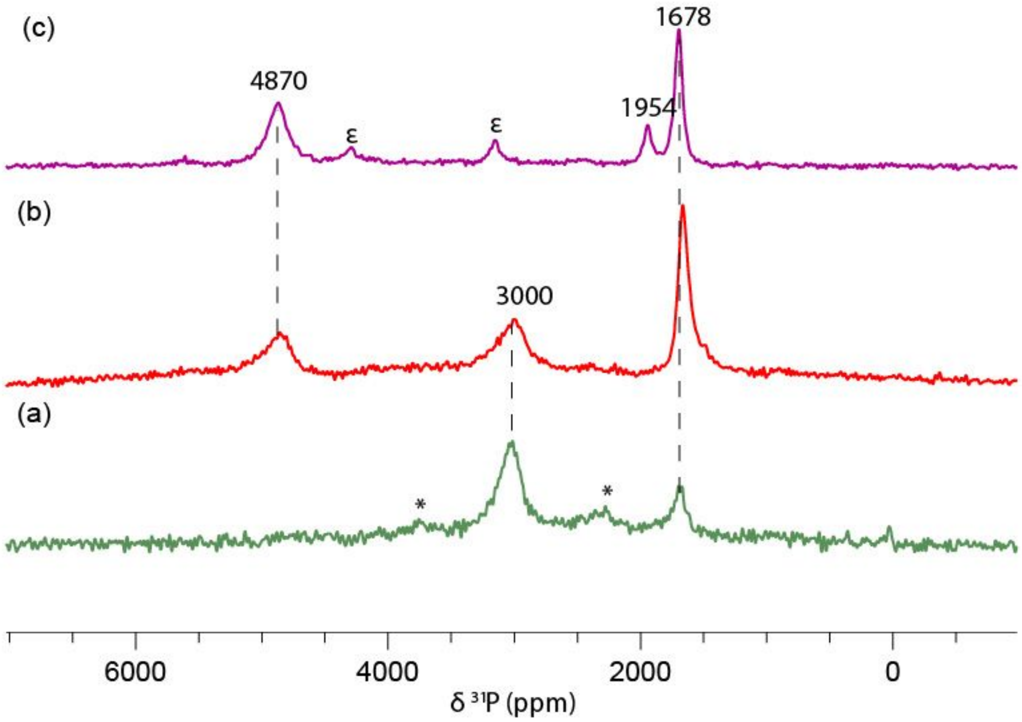

Figure 9. ^{31}P NMR spectra of (a) β-$LiVOPO_4$ discharged to 1.6 V, (b) β-$VOPO_4$ discharged to 1.6 V, and (c) chemically-lithiated β-Li_2VOPO_4. In (c), the peaks at ~4352 ppm and ~3160 ppm (marked as ε) are assigned to an ε-Li_2VOPO_4 impurity, while that at 1954 ppm is assigned to residual β-$LiVOPO_4$. Asterisks denote spinning sidebands.

2D NMR studies of Li ordering in Li_2VOPO_4

^7Li correlation experiments were carried out in order to narrow down the structure of the chemically-lithiated Li_2VOPO_4 from amongst all the structures generated from the convex hull for β-$LiVOPO_4$, which differ in their local lithium ordering. The 2D ^7Li POST-C7 spectrum of chemically lithiated β-Li_2VOPO_4 (Figure 10) shows the cross peaks between dipolar-coupled lithium environments in close spatial proximity to each other.

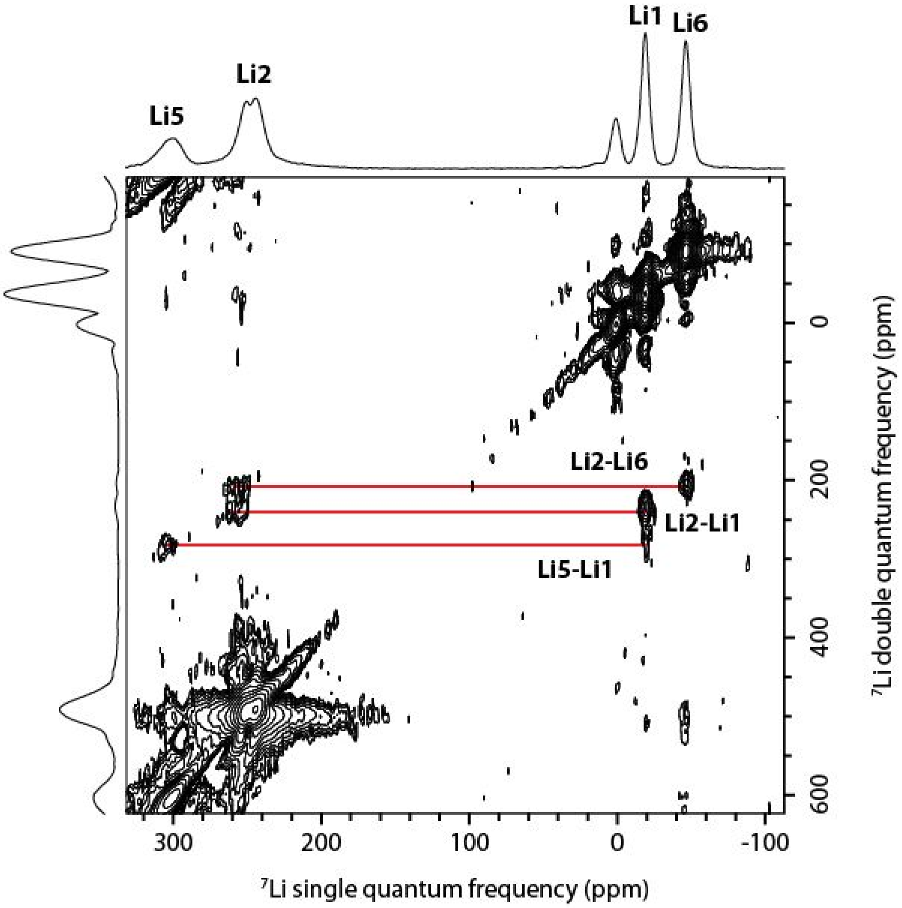

Figure 10. 2D ^{7}Li POST-C7 spectrum of chemically lithiated β-Li_2VOPO_4 acquired at 4.7 T with a MAS spinning frequency of 63 kHz, using excitation and reconversion periods of 286 μs each (9 basic POST-C7 elements). Red lines show the cross peaks between dipolar-coupled lithium environments in close spatial proximity. Skyline projections are shown on the top and left sides.

The POST-C7 spectrum (Figure 10) shows that the feature at −18 ppm (assigned to the more highly-coordinated Li1 site) is correlated to both of the distorted "tetrahedral" Li sites resonating at 255 ppm (Li2) and 306 ppm (Li5). (The site labels referred to here are as shown in Figure 2(d)). However, the other low-frequency resonance at −47 ppm (Li6) is correlated only to the Li at 255 ppm (Li2) and not to that at 306 ppm (Li5). In other words, considering all four possible correlations between the two distorted "tetrahedral" sites (Li5, Li2) and the more highly-coordinated sites (Li6, Li1), only the Li5–Li6 correlation is not observed; thus, we can conclude that the distance between these sites should be longer than the other Li–Li distances.

In agreement with the POST-C7 measurement, the 2D ^{7}Li EXSY spectrum (Figure 11) also indicates correlation of both of the lower-frequency features at −18 ppm (Li1) and −47 ppm (Li6) with the environment at 255 ppm (Li2). However, correlation of the more highly-coordinated environments to the distorted "tetrahedral" site at 306 ppm (Li5) is not observed in the EXSY, suggesting that this site is more disordered or further from these sites than is Li2. Based on the above assignments and comparing the Li–Li distances in the calculated structures, the experimental NMR spectrum for β-Li_2VOPO_4

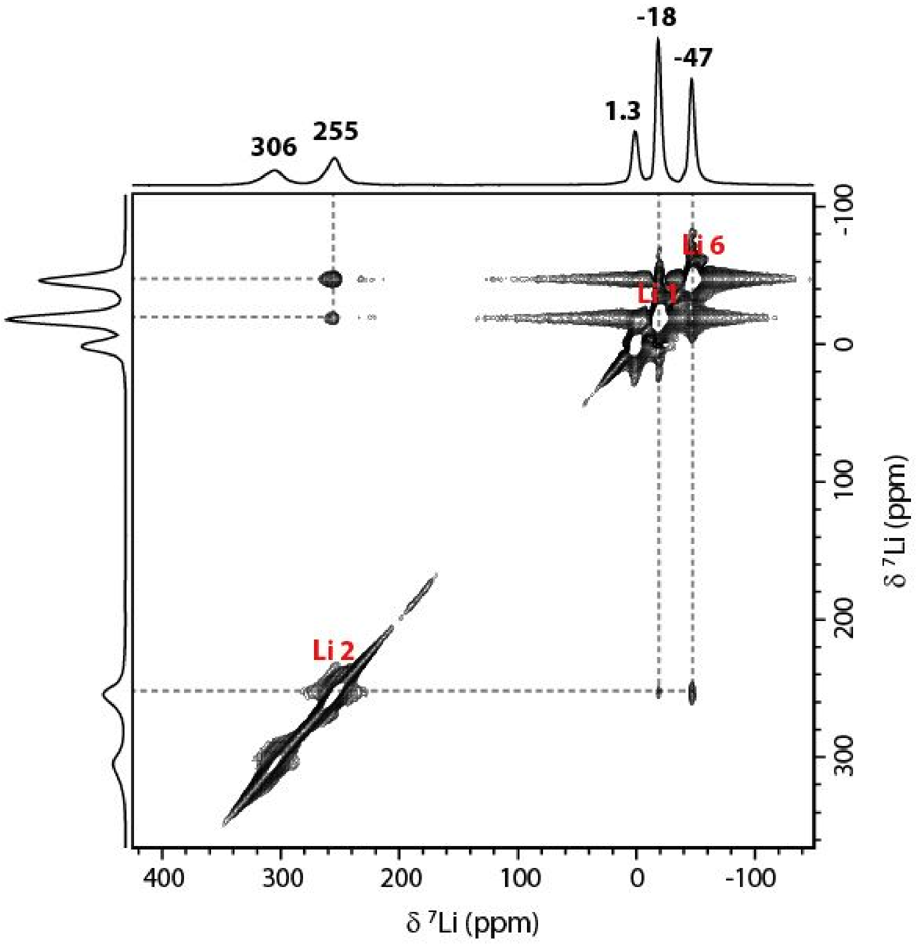

Figure 11. 2D ^{7}Li EXSY spectrum of chemically-lithiated β-$LiVOPO_4$, with a mixing period of 8 ms. The spectrum was acquired at a MAS frequency of 63 kHz at 4.7 T, using 720 t_1 increments of 8 μs. Off-diagonal cross peaks showing correlations between tetrahedral and octahedral Li sites are shown as dashed lines. Skyline projections are shown on the top and left sides.

best agrees with the calculated structure 2 given in Figure 2(d), which has a slightly higher energy than the lowest energy structure for β-Li_2VOPO_4. In particular, the Li5–Li6 distance (~3.5 Å) is considerably longer in calculated structure 2, in very good agreement with the result of the POST-C7 measurement where no correlation between the resonances from these sites is not observed. Key Li-Li distances are given in Table SI. 6 in the SI.

Metastability in this system:

Indication of the metastability of the intermediate phase β-$Li_{1.5}VOPO_4$ was assessed by recording the NMR spectrum of the electrochemically-lithiated sample discharged to 1.6 V after 3 months. This shows that the peak at ~60 ppm disappears and is accompanied by the growth of the peak at ~0 ppm indicating that over time the β-$Li_{1.5}VOPO_4$ phase transforms to β-$LiVOPO_4$ (Figure 12). Correspondingly, the ^{31}P shift at ~3000 ppm also disappears on aging the sample (SI.5) and this is consistent with this peak being assigned to the metastable β-$Li_{1.5}VOPO_4$ phase. On the other hand, the ^{31}P resonance at ~1600 ppm remains even after 3 months, consistent with this shift originating from the β-Li_2VOPO_4 phase rather than the metastable β-$Li_{1.5}VOPO_4$ phase.

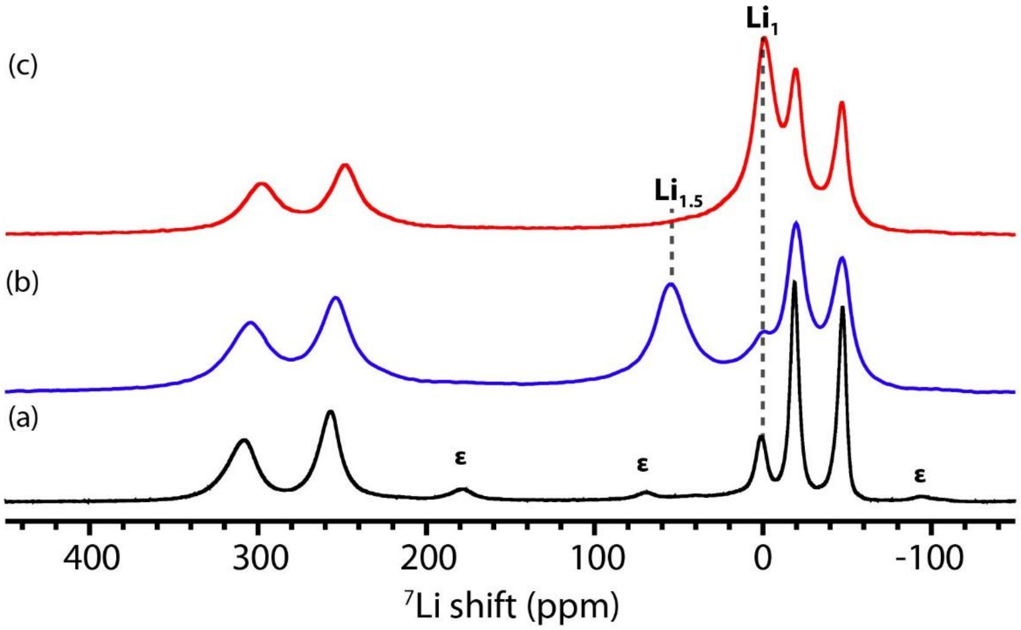

Figure 12. ^{7}Li NMR spectrum of (a) the chemically-lithiated β-Li_2VOPO_4 sample, compared with (b) β-$LiVOPO_4$ discharged to 1.6 V (electrochemically-lithiated β-Li_2VOPO_4), and (c) the spectrum of the sample shown in (b) after aging for 3 months. The minor peaks at ~178 ppm, 71 ppm and −93 ppm in the spectrum of chemically-lithiated β-Li_2VOPO_4 (labelled as ε) are assigned to a minor ε-Li_2VOPO_4 impurity.[47] Li_1 and $Li_{1.5}$ indicate NMR signatures characteristic of β-$LiVOPO_4$ and β-$Li_{1.5}VOPO_4$ phases respectively.

Discussion

The mechanism of electrochemical (de)lithiation in lithium-ion batteries is generally indicated by the nature of the galvanostatic charge-discharge curve, with a flat voltage profile indicating a two-phase reaction whereas a sloping curve indicates a solid solution mechanism. While the flat plateau in the discharge curve at 2.1 V suggests a two-phase reaction between β-$LiVOPO_4$ and β-Li_2VOPO_4, the presence of an intermediate phase of composition $Li_{1.5}VOPO_4$ was suggested by Lin et al who showed through DFT calculations that in addition to the $LiVOPO_4$ and Li_2VOPO_4 phases, both of which lie on the convex hull obtained for the phase diagram for $LiVOPO_4$, an additional phase, $Li_{1.5}VOPO_4$, also lies only slightly above the hull, indicative of a metastable phase (SI. 1. of Ref 31). Although no prior experimental evidence supports the formation of this intermediate phase, our NMR studies here show in the plateau region the formation of this intermediate, which is characterised by the ^{7}Li NMR resonance at ~60 ppm and the ^{31}P NMR resonance at ~3000 ppm of the samples cycled to a state of discharge corresponding to intercalation of ~0.5 Li. These NMR signatures are present even after discharging to 1.6 V indicating the persistence of this phase until the end of discharge and incomplete lithiation on electrochemical cycling. DFT calculations as given in Table 1 and Figure 3 support the assignment of these NMR features to the $Li_{1.5}$ phase.

In contrast, the chemically-lithiated β-Li_2VOPO_4 sample does not show NMR signatures indicative of the metastable β-$Li_{1.5}VOPO_4$ suggesting complete 2 Li intercalation on chemical lithiation. This difference in end products formed indicates that electrochemical intercalation is under kinetic control as a result of which the metastable $Li_{1.5}VOPO_4$ phase is formed in addition to the Li_2VOPO_4 phase when both the $LiVOPO_4$ as well as the $VOPO_4$ phase are discharged to 1.6 V. Chemical intercalation on the other hand is under thermodynamic control leading to the formation of only the stable Li_2VOPO_4 phase upon lithiation.

As the $Li_{1.5}VOPO_4$ phase and the Li_2VOPO_4 phases differ primarily in the nature of Li ordering while maintaining the same $VOPO_4$ connectivities, the expected XRD patterns of these phases are very similar (SI. 6 shows a simulation of the XRD patterns of these phases). Compounded by the often poor crystallinity of the intermediate phases obtained on cycling[10, 49], this would make the intermediate phases very difficult to distinguish from the end-member β-Li_2VOPO_4 phase by XRD.

The question still remains as to why there is no clear step in the voltage profile indicative of the β-$Li_{1.5}VOPO_4$ phase. This may be because the intermediate β-$Li_{1.5}VOPO_4$ phase lies very close to the hull in the β-$LiVOPO_4$- β-Li_2VOPO_4 phase diagram and therefore gives rise to a step in the voltage plateau that would be difficult to detect and likely masked by the huge overpotential observed on discharge between ~3.0 V and 2.0 V. However, the presence of a second small plateau at ~2.25 V on the charging curve supports the formation of this intermediate phase.

Conclusions

This paper demonstrates that electrochemically discharged β-$LiVOPO_4$ gives rise to metastable β-$Li_{1.5}VOPO_4$ intermediates in addition to the fully lithiated β-Li_2VOPO_4 phase. The formation of the metastable β-$Li_{1.5}VOPO_4$ phase, which lies close in energy to the convex hull between $LiVOPO_4$ and Li_2VOPO_4, does not lead to a clear step in the voltage plateau. However, solid state NMR experiments, supported by ab-initio DFT calculations, provide clear support for the formation and structure of this metastable phase as it gives rise to characteristic signatures in the ^{7}Li and ^{31}P NMR spectra. The metastable phases would be difficult to identify from other methods such as X-ray diffraction due to their poor crystallinity.

The 2D NMR ^{7}Li correlation experiments presented here were used to help deduce the complex Li ordering in chemically lithiated β-Li_2VOPO_4, the correlation experiments being used to select the most likely Li ordering candidate amongst several DFT-optimised structures. The methodology developed and the understanding gained therefrom will aid in the determination of complex Li orderings in other Li_xVOPO_4 polymorphs as well.

Acknowledgements

This work was supported as part of NECCES, an Energy Frontier Research Center funded by the U.S. Department of Energy, Office of Science, Office of Basic Energy Sciences under Award Number DE-SC0012583.
SB would like to thank Dr. Michael Hope (Cambridge) for useful NMR discussions.

References

(1) Mizushima, K.; Jones, P. C.; Wiseman. P. J.; Goodenough, J. B. Li_xCoO_2 ($0<x\leq1$): A new cathode material for batteries of high energy density. *Mater. Res. Bull.* **1980**, *15* (c), 783–789.

(2) Madhavi, S.; Rao, G. V. S.; Chowdari, B. V. R.; Li, S. F. Y. Effect of Aluminium Doping on Cathode Behaviour of $LiNi_{0.7}Co_{0.3}O_2$. *J. Power Sources* **2001**, *93*, 156–162.

(3) Lee, K. K.; Yoon, W. S.; Kim, K. B.; Lee, K. Y.; Hong, S. T. Characterization of $LiNi_{0.85}Co_{0.10}M_{0.05}O_2$ (M = Al, Fe) as a Cathode Material for Lithium Secondary Batteries. *J. Power Sources* **2001**, *97–98*, 308–312.

(4) Weaving, J. S.; Coowar, F.; Teagle, D. A.; Cullen, J.; Dass, V.; Bindin, P.; Green, R.; Macklin, W. J. Development of High Energy Density Li-Ion Batteries Based on $LiNi_{1-x-y}Co_xAl_yO_2$. *J. Power Sources* **2001**, *97–98*, 733–735.

(5) Guilmard, M.; Pouillerie, C.; Croguennec, L.; Delmas, C. Structural and Electrochemical Properties of $LiNi_{0.70}Co_{0.15}Al_{0.15}O_2$. *Solid State Ionics* **2003**, *160*, 39–50.

(6) Titov, A. A.; Eremenko, Z. V; Goryacheva, E. G.; Sokolova, N. P.; Opolchenova, N. L.; Stepareva, N. N.; Korobko, G. P. Synthesis, Structure, and Some Properties of $LiNi_{1/3}Co_{1/3}Mn_{1/3}O_2$. *Inorg. Mater.* **2013**, *49* (2), 202–208.

(7) Yabuuchi, N.; Ohzuku, T. Novel Lithium Insertion Material of $LiCo_{1/3}Ni_{1/3}Mn_{1/3}O_2$ for Advanced Lithium-Ion Batteries. *J. Power Sources* **2003**, *119–121*, 171–174.

(8) Liu, Z.; Yu, A.; Lee, J. Y. Synthesis and Characterization of $LiNi_{1-x-y}$ $Co_xMn_yO_2$ as the Cathode Materials of Secondary Lithium Batteries. *J. Power Sources* **1999**, *81–82*, 416–419.

(9) Li, J.; Zhang, Z. R.; Guo, X. J.; Yang, Y. The Studies on Structural and Thermal Properties of Delithiated $Li_xNi_{1/3}Co_{1/3}Mn_{1/3}O_2(0<x\leq1)$ as a Cathode Material in Lithium Ion Batteries. *Solid State Ionics* **2006**, *177* (2), 1509–1516.

(10) Padhi, A. K.; Nanjundaswamy, K. S.; Goodenough, J. B. Phospho-Olivines as Positive-Electrode Materials for Rechargeable Lithium Batteries. *J. Electrochem. Soc* **1997**, *144* (4).

(11) Hautier, G.; Jain, A.; Ong, S. P.; Kang, B.; Moore, C.; Doe, R.; Ceder, G. Phosphates as Lithium-Ion Battery Cathodes: An Evaluation Based on High-Throughput Ab Initio Calculations. *Chem. Mater.* **2011**, *23*, 3495–3508.

(12) Malik, R.; Abdellahi, A.; Ceder, G. A Critical Review of the Li Insertion Mechanisms in $LiFePO_4$ Electrodes. *J. Electrochem. Soc.* **2013**, *160* (5), A3179–A3197.

(13) Wang, J.; Sun, X. Olivine $LiFePO_4$: The Remaining Challenges for Future Energy Storage. *Energy Environ. Sci.* **2015**, *8* (4), 1110–1138.

(14) Yuan, L.; Wang, Z.; Zhang, W.; Hu, X.; Chen, J.; Huang, Y. Development and Challenges of $LiFePO_4$ Cathode Material for Lithium-Ion Batteries. **2011**, 269–284.

(15) Diaz, F.; Wang, Y.; Moorthy, T.; Friedrich, B. Degradation Mechanism of Nickel-Cobalt-Aluminum (NCA) Cathode Material from Spent Lithium-Ion Batteries in Microwave-Assisted Pyrolysis. *Metals (Basel).* **2018**, *8*, 565.

(16) Jung, S.-K.; Gwon, H.; Hong, J.; Park, K.-Y.; Seo, D.-H.; Kim, H.; Hyun, J.; Yang, W.; Kang, K. Understanding the Degradation Mechanisms of $LiNi_{0.5}Co_{0.2}Mn_{0.3}O_2$ Cathode Material in Lithium Ion Batteries. *Adv. Energy Mater.* **2014**, *4*, 1300787-.

(17) Keil, P.; Jossen, A. Calendar Aging of NCA Lithium-Ion Batteries Investigated by Differential Voltage Analysis and Coulomb Tracking. *J. Electrochem. Soc.* **2017**, *164* (1), A6066–A6074.

(18) Azmi, B. M.; Munirah, H. S.; Ishihara, T.; Takita, Y. Optimized $LiVOPO_4$ for Cathodes in Li-Ion Rechargeable Batteries. **2005**, *11*, 402–405.

(19) Azmi, B. M.; Ishihara, T.; Nishiguchi, H.; Takita, Y. Vanadyl Phosphates of $VOPO_4$ as a Cathode of Li-Ion Rechargeable Batteries. *J. Power Sources* **2003**, *119–121*, 273–277.

(20) Dupré, N.; Gaubicher, J.; Angenault, J.; Wallez, G.; Quarton, M. Electrochemical Performance of Different Li-$VOPO_4$ Systems. *J. Power Sources* **2001**, *98*, 532–534.

(21) Girgsdies, F.; Schneider, M.; Bruckner, A.; Ressler, T.; Schlogl, R. The Crystal Structure of δ-$VOPO_4$ and Its Relationship to ω-$VOPO_4$. *Solid State Sci.* **2009**, *11*, 1258–1264.

(22) Zhang, M.; Zhang, S.; Gao, H.; Meng, F. L.; Deng, C. Exploring High Performance $VOPO_4$ for Lithium Batteries : A Comparison between β and δ Polymorphs. *J.*

Electroanal. Chem. **2014**, *713*, 119–124.

(23) Gopal, R.; Calvo, C. Crystal Structure of β-VPO_5. *J. Solid State Chem.* **1972**, *5*, 432–435.

(24) He, G.; Bridges, C. A.; Manthiram, A. Crystal Chemistry of Electrochemically and Chemically Lithiated Layered α_I-$LiVOPO_4$. *Chem. Mater.* **2015**, *27* (19), 6699–6707.

(25) Lin, Y. C.; Wen, B.; Wiaderek, K. M.; Sallis, S.; Liu, H.; Lapidus, S. H.; Borkiewicz, O. J.; Quackenbush, N. F.; Chernova, N. A.; Karki, K.; Omenya, F.; Chupas, P. J.; Piper, L. F. J.; Whittingham, M. S.; Chapman, K. W.; Ong, S. P. Thermodynamics, Kinetics and Structural Evolution of ε-LiVOPO4 over Multiple Lithium Intercalation. *Chem. Mater.* **2016**, *28* (6), 1794–1805.

(26) Hameed, A. S.; Nagarathinam, M.; Reddy, M. V; Chowdari, B. V. R.; Vittal, J. J. Synthesis and Electrochemical Studies of Layer-Structured Metastable α_I-$LiVOPO_4$. *J. Mater. Chem.* **2012**, *22* (15), 7206–7213.

(27) Bianchini, M.; Ateba-Mba, J. M.; Dagault, P.; Bogdan, E.; Carlier, D.; Suard, E.; Masquelier, C.; Croguennec, L. Multiple Phases in the ε-VPO_4O–$LiVPO_4O$–Li_2VPO_4O System: A Combined Solid State Electrochemistry and Diffraction Structural Study. *J. Mater. Chem. A* **2014**, *2* (26), 10182.

(28) Ren, M. M.; Zhou, Z.; Gao, X. P. $LiVOPO_4$ as an Anode Material for Lithium Ion Batteries. *J. Appl. Electrochem.* **2010**, *40* (1), 209–213.

(29) Allen, C. J.; Jia, Q.; Chinnasamy, C. N.; Mukerjee, S.; Abraham, K. M. Synthesis, Structure and Electrochemistry of Lithium Vanadium Phosphate Cathode Materials. **2011**, *158* (12), 1250–1259.

(30) Harrison, K. L.; Bridges, C. A.; Segre, C. U.; Varnado, C. D.; Applestone, D.; Bielawski, C. W.; Paranthaman, M. P.; Manthiram, A. Chemical and Electrochemical Lithiation of $LiVOPO_4$ Cathodes for Lithium-Ion Batteries. *Chem. Mater.* **2014**, *26* (12), 3849–3861.

(31) Lin, Y.-C.; Hidalgo, M. F. V.; Chu, I.-H.;Chernova, N. A.; Whittingham, M. S.; Ong, S.-P. Comparison of the Polymorphs of $VOPO_4$ as Multi-Electron Cathodes for Rechargeable Alkali-Ion Batteries. *J. Mater. Chem. A* **2017**, *5*, 17421–17431.

(32) Hidalgo, M. F.; Lin, Y.-C.; Grenier, A.; D., X.; Rana, J.; Tran, R.; Xin, H.; Zuba, M.; Donohue, J.; Omenya, F. O.; Chu, I.-H.; Wang, Z.; Li, X.; Chernova, N. A.; Chapman, K. W.; Zhou, G.; Piper, L.; Ong, S.-P.; Whittingham, M. S. Rational Synthesis and Electrochemical Performance of $LiVOPO_4$ Polymorphs. *J. Mater. Chem. A* **2019**, *7*, 8423–8432.

(33) Lee, Y. K.; Kurur, N. D.; Helmle, M.; Johannessen, O. G.; Nielsen, N. C.; Levitt, M. H. Efficient Dipolar Recoupling in the NMR of Rotating Solids:A Sevenfold Symmetric Radiofrequency Pulse Sequence. *Chem. Phys. Lett.* **1995**, *242* (August), 304–309.

(34) Hohwy, M.; Jakobsen, H. J.; Edén, M.; Levitt, M. H.; Nielsen, N. C. Broadband Dipolar Recoupling in the Nuclear Magnetic Resonance of Rotating Solids : A Compensated C7 Pulse Sequence. *J. Chem. Phys.* **1998**, *108*, 2686–2694.

(35) Pourpoint, F.; Hua, X.; Middlemiss, D. S.; Adamson, P.; Wang, D.; Bruce, P. G.; Grey, C. P. New Insights into the Crystal and Electronic Structures of $Li_{1+x}V_{1-x}O_2$ from Solid State NMR, Pair Distribution Function Analyses, and First Principles Calculations. *Chem. Mater.* **2012**, *24*, 2880–2893.

(36) Jeener, J.; Meier, B. H.; Bachmann, P.; Ernst, R. R. Investigation of Exchange Processes by Two Dimensional NMR Spectroscopy. *J. Chem. Phys.* **1979**, *71*, 4546–4553.

(37) Abel, E. W.; Coston, T. P. J.; Orrell, K. G.; Sik, V.; Stephenson, D. Two-Dimensional NMR Exchange Spectroscopy. Quantitative Treatment of Multisite Exchanging

Systems. *J. Magn. Reson.* **1986**, *70*, 34–53.

(38) Davis, L. J. M.; He, X. J.; Bain, A. D.; Goward, G. R. Studies of Lithium Ion Dynamics in Paramagnetic Cathode Materials Using ^{6}Li 1D Selective Inversion Methods. *Solid State Nucl. Magn. Reson.* **2012**, *42*, 26–32.

(39) Dovesi, R.; Orlando, R.; Erba, A.; Zicovich-wilson, C. M.; Civalleri, B.; Casassa, S.; Maschio, L.; Ferrabone, M.; Pierre, M. D. La; Arco, P. D'; Noel, Y.; Causa, M.; Rerat, M.; Kirtman, B. CRYSTAL14: A Program for the Ab Initio Investigation of Crystalline Solids. *Int. J. Quantum Chem.* **2014**, *114*, 1287–1317.

(40) Adamo, C.; Barone, V. Toward Reliable Density Functional Methods without Adjustable Parameters: The PBE0 Model. *J. Chem. Phys.* **1999**, *110* (13), 6158–6170.

(41) Clément, R. J.; Pell, A. J.; Middlemiss, D. S.; Strobridge, F. C.; Miller, J. K.; Whittingham, M. S.; Emsley, L.; Grey, C. P.; Pintacuda, G. Spin-Transfer Pathways in Paramagnetic Lithium Transition-Metal Phosphates from Combined Broadband Isotropic Solid-State MAS NMR Spectroscopy and DFT Calculations. *J. Am. Chem. Soc.* **2012**, *134*, 17178–17185.

(42) Kim, J.; Middlemiss, D. S.; Chernova, N. A.; Zhu, B. Y. X.; Masquelier, C.; Grey, C. P.; Verne, J. Linking Local Environments and Hyperfine Shifts : A Combined Experimental and Theoretical 31 P and 7 Li Solid-State NMR Study of Paramagnetic Fe (III) Phosphates. *J. Am. Chem. Soc.* **2010**, *132*, 16825–16840.

(43) Middlemiss, D. S.; Ilott, A. J.; Clément, R. J.; Strobridge, F. C.; Grey, C. P. Density Functional Theory–Based Bond Pathway Decompositions of Hyperfine Shifts: Equipping Solid–State NMR to Characterize Atomic Environments in Paramagnetic Materials. *Chem. Mater.* **2013**, *25*, 1723–1734.

(44) Zhang, Y.; Castets, A.; Carlier, D.; Menetrier, M.; Boucher, F. Simulation of NMR Fermi Contact Shifts for Lithium Battery Materials : The Need for an Efficient Hybrid Functional Approach. *J. Phys. Chem. C* **2012**, *116*, 17393–17402.

(45) Shi, Y.; Zhou, H.; Seymour, I. D.; Britto, S.; Rana, J.; Wangoh, L. W.; Huang, Y.; Yin, Q.; Reeves, P. J.; Zuba, M.; Chung, Y.; Omenya, F.; Chernova, N. A.; Zhou, G.; Piper, L. F. J.; Grey, C. P.; Whittingham, M. S. Electrochemical Performance of Nanosized Disordered $LiVOPO_4$. *ACS Omega* **2018**, *3*, 7310–7323.

(46) Lii, K, H.; Li, C, H.; Cheng, C.Y.; Wang, S. L. Hydrothermal Synthesis, Structure, and Magnetic Properties of a New Polymorph of Lithium Vanadyl (IV) Orthophosphate: β-$LiVOPO_4$. *J. Solid State Chem.* **1991**, *95*, 352–359.

(47) Siu, C.; Seymour, I. D.; Britto, S.; Zhang, H.; Rana, J.; Feng, J.; Omenya, F. O.; Zhou, H.; Chernova, N. A.; Guangwen, Z.; Grey, C. P.; Piper, L. F. J.; Whittingham, M. S. Enabling Multi-Electron Reaction of ε-$VOPO_4$ to Reach Theoretical Capacity for Lithium-Ion Batteries. *Chem. Commun. (Camb).* **2018**, *54*, 7802–7805.

(48) Whittingham, M. S.; Dines, M. B. N-Butyllithium-An Effective, General Cathode Screening Agent. *J. Electrochem. Soc.* **1977**, *124* (9), 1387–1388.

(49) He, G.; Kan, W.-H.; Manthiram, A. Delithiation/Lithiation Behaviours of Three Polymorphs of $LiVOPO_4$. *Chem. Commun. (Camb).* **2018**, *54*, 13224–13227.

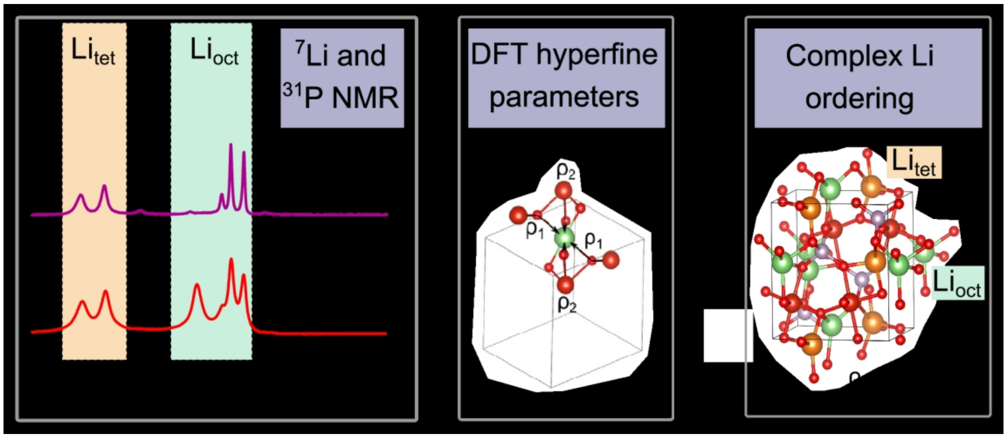

Li_{tet}
Li_{oct}
^{7}Li and ^{31}P NMR
DFT hyperfine parameters
ρ$_1$
ρ$_1$
ρ$_2$
ρ$_2$
Complex Li ordering
Li_{tet}
Li_{oct}